Development 140, 385-394 (2013) doi:10.1242/dev.083683


# GPI biosynthesis is essential for rhodopsin sorting at the *trans*-Golgi network in *Drosophila* photoreceptors

**Takunori Satoh[1], Tsuyoshi Inagaki[2], Ziguang Liu[1], Reika Watanabe[3] and Akiko K. Satoh[1,*]**

## SUMMARY

Sorting of integral membrane proteins plays crucial roles in establishing and maintaining the polarized structures of epithelial cells and neurons. However, little is known about the sorting mechanisms of newly synthesized membrane proteins at the *trans*-Golgi network (TGN). To identify which genes are essential for these sorting mechanisms, we screened mutants in which the transport of Rhodopsin 1 (Rh1), an apical integral membrane protein in *Drosophila* photoreceptors, was affected. We found that deficiencies in glycosylphosphatidylinositol (GPI) synthesis and attachment processes cause loss of the apical transport of Rh1 from the TGN and mis-sorting to the endolysosomal system. Moreover, $Na^+K^+$-ATPase, a basolateral membrane protein, and Crumbs (Crb), a stalk membrane protein, were mistransported to the apical rhabdomeric microvilli in GPI-deficient photoreceptors. These results indicate that polarized sorting of integral membrane proteins at the TGN requires the synthesis and anchoring of GPI-anchored proteins. Little is known about the cellular biological consequences of GPI deficiency in animals *in vivo*. Our results provide new insights into the importance of GPI synthesis and aid the understanding of pathologies involving GPI deficiency.

**KEY WORDS: GPI, Rhodopsin, Sorting, *Drosophila***

## INTRODUCTION

The biosynthesis of glycosylphosphatidylinositol (GPI)-anchored proteins has been thoroughly investigated in cultured cells and yeast for 20 years, resulting in the identification of a number of genes involving GPI anchoring, with names originating from PIG, phosphatidylinositol glycan (Fujita and Kinoshita, 2010; Maeda and Kinoshita, 2011). However, little is known about the phenotypic consequences of dysfunction in the GPI pathway *in vivo*. Knockout of *Pig-a* (*Piga* – Mouse Genome Informatics), a component of GPI-GlcNAc transferase and the enzyme at the first step of GPI biosynthesis, causes embryonic lethality in mice (Nozaki et al., 1999). Somatic mutations in the *PIG-A* (*PIGA* – Human Gene Nomenclature Database) gene in hematopoietic stem cells are associated with paroxysmal nocturnal hemoglobinuria (Takeda et al., 1993). A hypomorphic promoter mutation in *PIGM*, a mannosyltransferase-encoding gene, causes venous thrombosis and seizures (Almeida et al., 2006). *PIGV*, which encodes α1,6-mannosyltransferase II, was identified as the gene mutated in hyperphosphatasia mental retardation (Krawitz et al., 2010). As expected, deficient GPI anchoring or remodeling causes lost or delayed transport or secretion of GPI-anchored proteins. Furthermore, recent studies in yeast and zebrafish show that the transport of non-GPI-anchored proteins is also affected by abolishment of GPI biosynthesis (Okamoto et al., 2006; Nakano et al., 2010).

*Drosophila* photoreceptors are well suited for studying polarized transport, because a single retinal cross section simultaneously shows three distinct plasma membrane domains of numerous photoreceptors (Fig. 1A-C). One is the photoreceptive membrane domain, known as the rhabdomere, which is formed at the center of the apical plasma membrane as a column of closely packed rhodopsin-rich photosensitive microvilli (Fig. 1B,C). The second is the peripheral apical domain surrounding the rhabdomere, termed the stalk membrane, where Crb and β-spectrin are enriched (Izaddoost et al., 2002; Pellikka et al., 2002). The third is the basolateral membrane, which is separated from apical membrane by adherens junctions, similarly to the typical polarized epithelial cells. $Na^+K^+$-ATPase specifically localizes on the basolateral membrane (Yasuhara et al., 2000). In addition to these three membrane domains, fly photoreceptors possess a fourth domain, the axon and synapses, which extend below the retina to the brain (not shown).

Rhodopsin 1 (Rh1), the rhodopsin expressed in R1-R6 cells, the major retinal photoreceptor cells, is the most accessible protein for investigating apical polarized transport in fly photoreceptors. This is because it is massively synthesized and transported in the late pupal stage (Kumar and Ready, 1995) and its exit from the endoplasmic reticulum (ER) can be triggered by illumination with blue light (Ozaki et al., 1993). We and other groups have shown that Rab1 is involved in transport from the ER to the Golgi (Satoh et al., 1997), Rab6 works in the early transport pathway (Shetty et al., 1998), the Rab11-Rip11-MyoV (Didum – FlyBase) complex is essential for the post-Golgi transport of Rh1 (Satoh et al., 2005; Li et al., 2007), and the exocyst complex is essential for the tethering of post-Golgi vesicles to the base of the rhabdomeres (Beronja et al., 2005). To elucidate further the molecular mechanism of Rh1 transport, we screened for mutants deficient in Rh1 transport and found that PIG genes are essential for Rh1 transport. Our analysis of Rh1 transport in GPI-deficient cells revealed that GPI anchoring is essential for the polarized sorting of integral membrane proteins at the *trans*-Golgi network (TGN).

## MATERIALS AND METHODS

### *Drosophila* stocks and genetics

Flies were grown at 20-25°C in a 12-hour light/12-hour dark environment on standard cornmeal-glucose-agar-yeast food unless noted

[1]Division of Life Science, Graduate School of Integral Arts and Science, Hiroshima University, 1-7-1 Kagamiyama, Higashi-hiroshima 739-8521, Japan. [2]Radiological Imaging and Informatics, Health Sciences, Graduate School of Medicine, Tohoku University, 2-1 Seiryo-machi, Aoba-ku, Sendai 980-8575, Japan. [3]Department of Biochemistry Sciences II, University of Geneva, 30 quai Ernest-Ansermet, 1211 Geneva, Switzerland.

*Author for correspondence (aksatoh@bio.nagoya-u.ac.jp)

**Accepted 22 October 2012**

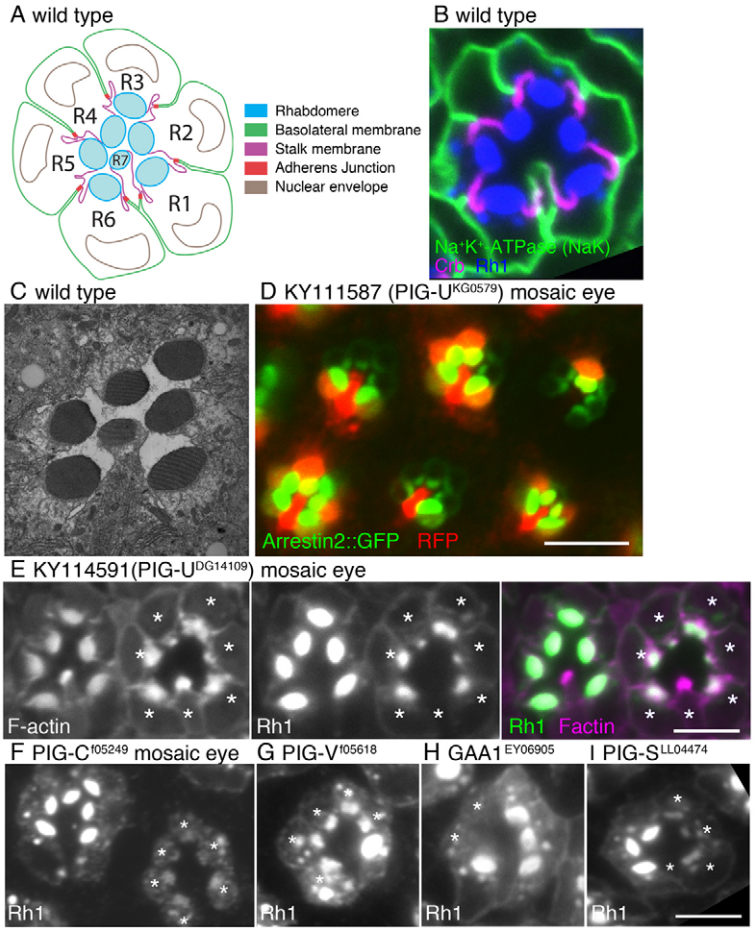


**Fig. 1. Screening and identification of PIG genes as essential components for Rh1 transport.** (**A**) Schematic view of a *Drosophila* ommatidium cross section showing three different plasma membrane domains for each photoreceptor. (**B**) Immunostaining of an ommatidial cross section. Three membrane proteins, Rh1 (blue), Crb (purple) and $Na^+K^+$-ATPase (green), are localized on the different membrane domains. (**C**) Electron microscopic cross section of an ommatidium. (**D**) KY111587 mosaic retina. RFP (red) marks wild-type cells; RFP expression levels in each cell are variable. Arrestin2::GFP (green) shows endogenous Rh1 localization. Scale bar: 10 μm. (**E**) KY114591 mosaic retina was stained by Rh1 (green) and F-actin (magenta). Asterisks show mutant photoreceptors. Scale bar: 5 μm. (**F-I**) Rh1 immunostaining of a cross section of an ommatidium from PIG-null mosaic eyes. Asterisks show PIG-null photoreceptors. Scale bar: 5 μm.

otherwise. Carotenoid-deficient food was prepared from 1% agar, 10% dry yeast, 10% sucrose, 0.02% cholesterol, 0.5% propionate and 0.05% methyl 4-hydroxybenzoate. The fly stocks obtained from Bloomington (BL), the Kyoto *Drosophila* Genetic Resource Center (KY) or Harvard (HV) stock centers are referred to with their respective sources and stock numbers.

To visualize the genetic mosaic on the retina, *3xP3-RFP* transgenes (Bischof et al., 2007), which express red fluorescent protein (RFP) in photoreceptors under the control of an artificial *3xP3* promoter, were recombined with proximal *neoFRT* transgenes on the same chromosome arm as follows: *M{3xP3-RFP.attP}ZH-2A* (BL24480) and *neoFRT19A*; *M{3xP3-RFP.attP′}ZH-22A* (BL24481) and *neoFRT40A*; *M{3xP3-RFP.attP′}ZH-58A* (BL24484) and *neoFRT42D*; *M{3xP3-RFP.attP′}ZH-68E* (BL24485) and *neoFRT80B*; and *M{3xP3-RFP.attP′}ZH-96E* (BL24487) and *neoFRT82B*. The following test lines were used for live-image screening: *y w P3RFP FRT19A; Rh1Arr2GFP eye-FLP/SM1, w; P3RFP FRT40A/SM1; Rh1Arr2GFP eye-FLP/TM6B, w; FRT42D P3RFP; Rh1Arr2GFP eye-FLP/TM6B, w; Rh1Arr2GFP eye-FLP/SM1; P3RFP FRT80B, w; Rh1Arr2GFP eye-FLP/SM1;* and *FRT82B P3RFP*. Similar fly stocks without *Rh1Arr2GFP* transgene were used for the immunostaining of mosaic retina.

To generate deletion mutants of *PGAP3* by imprecise excision, a P-element insertion on the 5′ of *PGAP3* gene, *P{SUPor-P}[KG03595]*(BL13019), was outcrossed to w1118 six times and subsequently excised using *delta2-3* (BL3629). The deletion was analyzed by PCR using KOD-FX DNA polymerase and the primers 5′-TGCGAAAACACAGAAACTGC-3′ and 5′-TCGATATAACCGGCTT-GTGA-3′.

*GlcT-1* deletion mutants were generated using a standard induced FLP/FRT recombination method (Parks et al., 2004). Trans-heterozygous males of *PBac(RB)$^{e2597}$* (HVe2597) and *FRT42D PBac(RB)$^{e2644}$* (KY114503) carrying *hs-FLP* (BL6876) were heat treated three times at 37°C for 1 hour during their larval stages. *SM6a*-balanced offspring were genotyped using PCR to select recombinants carrying both the proximal side of *e2644* and the distal side of *e2597* with the following primers: 5′-TATTTTGCTGGGTTCCGAGT-3′ and 5′-TCCAAGCGGCGACTGA-GATG-3′ for e2644, and 5′-CCTCGATATACAGACCGATAAAAC-3′ and 5′-GTAGAAGGTGCCCGAGTTGA-3′ for e2597.

Coding insertions of *PIG-C pBac{WH}$^{f05249}$* (HVf05249), *PIG-V PBac{WH}$^{f05618}$* (HVf05618), *GAA1 P{EPgy2}$^{EY06905}$* (BL17363), *PIG-S P{GSV6}$^{GS12695}$* (KY205476) and *PGAP5 Mi{ET1}$^{MB11752}$* (BL29250) were recombined by meiotic recombination with *FRT80B*, *FRT42D*, *FRT19A*, *FRT82B* and *FRT40A*, respectively. Mosaic retinas were visualized by mating with *3xP3RFP-FRT* chromosomes, except *PGAP5 $^{MB11752}$*, which has a *3xP3-GFP* marker.

For the partial rescue experiment, the entire coding sequence of the *PIG-C* (*PIGC* – Human Gene Nomenclature Database) gene was cloned into *pPTW* to construct *pP{UAS-PIG-C}* and transgenic lines were generated by BestGene (Chino Hills, CA, USA)

### Live-image screening

Each mutant line obtained from the Kyoto *Drosophila* Genetic Resource Center (DGRC) (supplementary material Table S1) was mated with the test lines. Late pupae of the siblings were attached to glass slides using double-sided sticky tape, and the pupal cases around the heads were removed. The pupae were chilled on ice, embedded in 0.2-0.5% agarose, and observed using an FV1000 confocal microscope equipped with LUMPlanFI water-immersion 40× objective (Olympus, Tokyo, Japan).

### Live imaging of fluorescent proteins expressed in photoreceptors

For live-image screening, mutant flies obtained from the Kyoto DGRC were mated with the test lines carrying *FRT*, *3xP3-RFP*, *eye-FLP* and *Rh1Arr2GFP*.

#### Construction of the antibody against *Drosophila* Rh1

Chicken affinity-purified anti-Rh1 antibody was raised against the Rh1 peptide GSVVDKVTPDMAHLIS (amino acids 21-36) (BioGate, Gifu, Japan). The antibody recognizes the band of Rh1 in western blots, previously identified by another anti-Rh1 monoclonal antibody, 4C5.

#### Immunohistochemistry

Fixation and staining were performed as described previously (Satoh and Ready, 2005). Primary antisera were as follows: mouse monoclonal anti-Rh1 [4C5; 1:20 supernatant; Developmental Studies Hybridoma Bank (DSHB), Iowa, IA, USA], rabbit anti-Rh1 (1:1000) (Satoh et al., 2005), chicken anti-Rh1 (1:1000; made in the present study), rabbit anti-GM130 (1:300; Abcam, Cambridge, UK), rabbit anti-NinaA (1:300; gift from Dr Zuker, Columbia University, NY, USA), mouse monoclonal anti-$Na^+K^+$-ATPase alpha subunit (1:500 ascites; DSHB), rat monoclonal anti-DE-Cad (1:20 supernatant; DSHB), mouse monoclonal anti-Chp (24B10; 1:20 supernatant; DSHB), mouse monoclonal anti-Arm (1:20 supernatant; DSHB), rat anti-Crb (gift from Dr Tapass, University of Toronto, ON, Canada), rabbit anti-transient receptor potential (TRP; gift from Dr Montell, the Johns Hopkins University, MD, USA), rabbit anti-Rab7 (1:1000) and rat anti-Rbsn5 (1:1000; gift from Dr Nakamura, Riken, Kobe, Japan). The secondary antibodies were anti-mouse, anti-rabbit, anti-rat and anti-chicken labeled with Alexa Fluor 488, 568 or 647 (1:300; Invitrogen, Carlsbad, CA, USA) with or Cy2 (1:300; GE Healthcare Life Sciences, Pittsburgh, PA, USA). Samples were examined using an FV1000 confocal microscope (60×1.42-NA lens) and images were recorded. To minimize bleed through, each signal in double- or triple-stained samples was imaged sequentially. Images were processed in accordance with the guidelines for proper digital image handling using Image J and/or Adobe Photoshop CS3.

#### Filipin staining

Filipin (1 mg; Sigma-Aldrich, St Louis, MO, USA) was dissolved in 400 µl DMSO (2.5 mg/ml) as a stock solution. Eyes were fixed and washed with 1× PBS and stained with 50 µg/ml filipin and Alexa Fluor 488-conjugated phalloidin (Invitrogen) for 2 hours and observed using an LSM710 confocal microscope (Carl Zeiss, Oberkochen, Germany).

#### Blue light-induced chromophore supply (BLICS) method

Newly eclosed flies fed carotenoid-deficient food were transferred to carotenoid-deficient food with crystalline all-*trans* retinal (Sigma-Aldrich) in the dark. After 1 or 2 days in the dark, the flies were irradiated with blue light (410 nm) using a CFP filter on a 75-W xenon lamp to isomerize the all-*trans* retinal to the 11-*cis*-form and initiate Rh1 maturation.

#### Electron microscopy

The conventional electron microscopic methods used are described by Satoh et al. (Satoh et al., 1997). Samples were observed on JEM1200 and JEM1400 electron microscopes (JEOL, Tokyo, Japan).

#### Preparation of detergent-resistant fraction

A detergent-resistant membrane was prepared using a rapid method as described previously (Adam et al., 2008). Preparation was carried out at 4°C in buffer-A (30 mM NaCl, 5 mM EDTA and 20 mM HEPES; pH 7.5) containing 1:200 Protease Inhibitor Mix III (Calbiochem). Total membranes were prepared from the pupal heads of *Rip11* dominant-negative mutants (w; *Rh1-Gal4/UAS-dRip11-DN-GFP*) or frozen heads of 0- to 1-day-old w1118 adults. The heads were homogenized in buffer-A using Biomasher II (Assist, Tokyo, Japan). The homogenates were centrifuged at 860 ***g*** for 3 minutes to remove the cuticle. The supernatants were centrifuged at 21,500 ***g*** for 30 minutes to collect the total membrane fraction. About 40 µl precipitated membranes was resuspended in 60 µl buffer-A, mixed with an equal volume of 2% Triton-X in buffer-A, and incubated on ice for 1 hour. The lysates were centrifuged at 21,500 ***g*** for 30 minutes to separate detergent-resistant and detergent-soluble fractions, then dissolved in sodium dodecyl sulfate sample buffer to a final volume of 100 µl. The fractions were then analyzed by immunoblotting 10 µl each for anti-TRP and 4C5 monoclonal anti-Rh1 antibodies.

#### Immunoblotting

Immunoblotting was performed as described previously (Satoh et al., 1997). The following antibodies were used: mouse monoclonal anti-TRP (1:3000; DSHB) and mouse monoclonal anti-Rh1 (4C5; 1:5000 concentrated supernatant; DSHB) as primary antibodies and HRP-conjugated anti-mouse antibody (1:20,000, Jackson ImmunoResearch Laboratories) as a secondary antibody. Primary antibodies were incubated overnight at 4°C, and secondary antibody incubation and washing were performed using the SNAP-id Protein Detection System (Millipore, Billerica, MA, USA). Signals were visualized using enhanced chemiluminescence (ECL; GE Healthcare Life Sciences).

## RESULTS

### Live-image screening of mutants exhibiting Rh1 transport defects in fly photoreceptors

To identify which genes are essential for Rh1 transport, we performed retinal mosaic screening using the FLP/FRT method (Xu and Rubin, 1993) and two-color fluorescence imaging, similar to a method described recently (Gambis et al., 2011). In our screening, RFP was used as a wild-type cell marker and Arrestin2::GFP (Satoh et al., 2010) was used to visualize endogenous Rh1 localization. The cornea neutralization technique was applied to observe the phenotype *in vivo* (supplementary material Fig. S1A,B) (Mollereau et al., 2000; Pichaud and Desplan, 2001). As Arrestin2::GFP was expressed in all R1-R6 peripheral photoreceptors in the mosaic retina, the localization and amounts of Rh1 could be compared between wild-type and mutant cells within the same optical section.

We screened 546 lines of lethal insertions of *P-element* or *piggyBac* transposons in the University of California, Los Angeles Undergraduate Research Consortium in Functional Genomics (UCLA URCFG) collection (Chen et al., 2005) using the two-color live-imaging method (supplementary material Table S1). For selected lines that showed some deficiency, the distributions of Rh1 and $Na^+K^+$-ATPase were investigated by immunostaining to observe the phenotypes of transport and morphogenesis. Among the lines exhibiting severe Arrestin2::GFP reduction with only minor ommatidial disorganization, two lines, KY111587 (Fig. 1D) and KY114591 (data not shown), had an insertion on the 5′ UTR or promoter region of a particular gene, *CG13089*. Immunostaining of these two mosaic retinas with anti-Rh1 revealed a dramatic reduction of Rh1 in the rhabdomeres (Fig. 1E; data not shown). This phenotype was rescued by the removal of the *P-element* insertion in both lines (supplementary material Fig. S1C,D), indicating that the Rh1 reduction is caused by the reduction of *CG13089* gene function. *CG13089* has 38% identity and 57% similarity to the human *PIG-U* (*PIGU* – Human Gene Nomenclature Database) gene, which encodes a subunit of GPI-transamidase (supplementary material Table S2). As Rh1 is an integral membrane protein and is not anchored by GPI, these results suggest that the formation of GPI-anchored proteins is also important for the trafficking of non-GPI-anchored proteins to the rhabdomeres.

### Roles of GPI synthesis and remodeling in Rh1 transport

The *PIG-U* alleles identified in our screening are hypomorphic; no *PIG-U*-null mutant was available. To investigate further the role of GPI synthesis and anchoring *in vivo*, we searched for null mutants of other PIG genes in the genome of *Drosophila melanogaster* (supplementary material Table S2). There were four available insertions in the coding regions of PIG genes: $PIG\text{-}C^{f05249}$, $PIG\text{-}V^{f05618}$, $GAA1^{EY069050}$ and $PIG\text{-}S^{LL04474}$ (supplementary material Fig. S1E).

As all four null mutants are embryonic (i.e. *PIG-S*$^{LL04474}$) or larval lethal (i.e. *PIG-C*$^{f05249}$, *PIG-V*$^{f05618}$ and *GAA1*$^{EY06905}$), we recombined them with *FRT* chromosomes to make mosaic retinas. We first investigated Rh1 localization in *PIG*-null homozygous clones (Fig. 1F-I). The severe reductions of Rh1 in *PIG-C*$^{f05249}$, *PIG-S*$^{LL04474}$ and *GAA1*$^{EY06905}$ mutant cells (asterisks) indicate that GPI synthesis and/or anchoring is essential for Rh1 synthesis or transport. *PIG-V*$^{f05618}$ mutant photoreceptors exhibited less Rh1 reduction in the rhabdomeres than any other allele tested. The mutant clone sizes in *PIG-V*$^{f05618}$ mutant retinas were larger than those of the other three null mutants: >13% of ommatidia in *PIG-V*$^{f05618}$ mosaics were composed of only mutant cells compared with <3% in the other three mutants (supplementary material Fig. S1E). These results are concordant with the smaller Rh1 transport deficit observed in *PIG-V*$^{f05618}$ mutants relative to that in the other three nulls. The loss of PIG-V activity in humans results in reduced anchoring of alkaline phosphatase (ALP) to the surface membrane and elevated ALP activity in blood serum (Krawitz et al., 2010). The recent explanation for this phenomenon states that GPI transamidase recognizes incomplete GPI-bearing mannose and cleaves a hydrophobic signal peptide, resulting in the secretion of soluble ALP (Murakami et al., 2012). Similarly, proteins having partial functioning without GPI anchoring might be released from the ER to the secretory pathway in fly *PIG-V*$^{f05618}$ mutant photoreceptors, which could result in the milder phenotype of the *PIG-V* null mutant. A recent study on *PIG-V* shows a similar but milder Rh1 reduction in *PIG-V*$^{A276V}$, which has an alanine-to-valine substitution at amino acid position 276V (Rosenbaum et al., 2012).

The structures of the lipid and glycan moieties on GPI anchors are remodeled during biosynthesis and after attachment to proteins (Fujita and Kinoshita, 2010). Lipid remodeling is required for the proper transport and raft association of GPI-anchored proteins (Maeda and Kinoshita, 2011). The proteins involved in these processes are called post-GPI attachment proteins (PGAPs) (supplementary material Fig. S1F). We searched the genomic sequences of *D. melanogaster* for *PGAP* genes and found a lethal insertion, *PGAP5*$^{MB11752}$, containing a transposon insertion in exon 2 of *PGAP5* (supplementary material Table S2). We recombined *PGAP5*$^{MB11752}$ onto the *FRT40A* chromosome and investigated Rh1 localization in mosaic clones. Unexpectedly, Rh1 localized normally in rhabdomeres in *PGAP5*-null photoreceptors (supplementary material Fig. S1G). To obtain a *PGAP3*-null mutant, we created deletion mutants of the *PGAP3* gene using imprecise excision of a *P-element* insertion, *PGAP3*$^{KG03595}$ (supplementary material Fig. S1H). We obtained two *PGAP3*-null mutants, *PGAP3*$^{\Delta 4B3}$ and *PGAP3*$^{\Delta 3F10}$; both were homozygous viable and exhibited normal Rh1 localization (supplementary material Fig. S1I; data not shown). These results indicate that GPI synthesis but not GPI remodeling is essential for Rh1 delivery to the rhabdomere.

## Chaoptin accumulation in the ER of GPI-deficient photoreceptors

As GPI-anchored proteins are expected to be not synthesized normally or to be secreted rather than binding to the membrane in GPI-deficient cells, we investigated the synthesis and transport of Chaoptin (Chp), a major GPI-anchored protein in fly photoreceptors (Krantz and Zipursky, 1990). In wild-type cells, Chp localizes at the rhabdomere. However, in GPI-deficient cells, most Chp colocalizes with the Rh1 chaperone NinaA (Colley et al., 1991) in the ER; only a limited amount of Chp was detected in the rhabdomeres (Fig. 2A). Although GPI-free Chp was expected to be secreted, no Chp secretion to the inter-rhabdomeric space (IRS) was observed in any PIG mutant. These observations indicate that GPI anchoring is essential for the ER exit of Chp. However, Chp localized normally to the rhabdomeres of both *PGAP3* and *PGAP5* mutant photoreceptors (data not shown), suggesting that GPI remodeling is not essential for Chp synthesis or transport.

## Rhabdomeric membrane in PIG mutant photoreceptors

Electron microscopic observations of thin sections revealed that rhabdomeres in GPI-deficient photoreceptors were severely disrupted (Fig. 2B). In wild-type photoreceptors, rhabdomere microvilli were tightly packed and rhabdomeres had round cross-

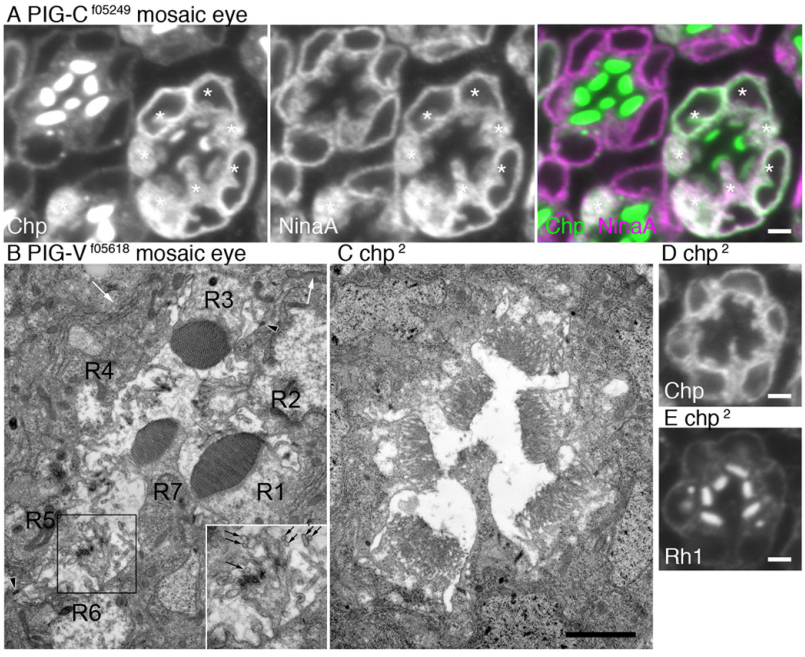


**Fig. 2. Essential roles of PIG genes in Chp transport and rhabdomere formation.** (**A**) *PIG-C*$^{f05249}$ mosaic *Drosophila* eye immunostained by anti-Chp (green) and anti-NinaA antibodies (magenta). Asterisks show *PIG-C*-null photoreceptors. (**B**) *PIG-V*$^{f05618}$ mosaic ommatidium by electron microscopy. R1, R3 and R7 photoreceptors are wild type; R2, R4, R5 and R6 photoreceptors are *PIG-V*-null mutants. Adherens junctions (arrowheads) and basolateral membrane (white arrows) are indicated. Inset: High-magnification image of an R6 rhabdomere; black arrows show cross sections of the microvilli. (**C**) *chp*$^{2}$ mutant ommatidium by electron microscopy. (**D**) Chp immunostaining of *chp*$^{2}$ mutant ommatidium. (**E**) Rh1 immunostaining of *chp*$^{2}$ mutant ommatidium. Scale bars: 2 μm.

sectional profiles. However, the rhabdomeres of GPI-deficient cells were small and irregularly shaped; the number of microvilli was greatly reduced, and the microvilli had different orientations and were not packed tightly (Fig. 2B, inset). Some microvilli in GPI-deficient photoreceptors had greater diameters and shorter lengths than the wild-type microvilli (Fig. 2B, black arrows in inset). Adherens junctions and the basolateral membrane (Fig. 2B, arrowheads and white arrows, respectively; supplementary material Fig. S2) as well as cytoplasmic organelles, the ER, Golgi bodies and mitochondria were normal (supplementary material Fig. S2). Therefore, the apical plasma membrane, especially the central rhabdomere domain, was specifically disrupted in GPI-deficient photoreceptors.

As shown in Fig. 2A, GPI-deficient rhabdomeres lacked Chp, which packs rhabdomere microvilli through homotypic adhesion (Reinke et al., 1988). An allele of *chp*, $chp^2$, encodes a truncated form of Chp that lacks the GPI-attachment site (Krantz and Zipursky, 1990). This Chp N-terminal polypeptide in the $chp^2$ mutant was retained in the ER and was not transported to the rhabdomeres (Fig. 2D). The microvilli in $chp^2$ mutants are relatively short, have variable length and are separated from each other (Fig. 2C) as described previously (Krantz and Zipursky, 1990). However, the morphology of $chp^2$ mutant rhabdomeres was much less impaired than that of GPI-deficient photoreceptors. Most importantly, $chp^2$ mutants showed only a mild reduction of Rh1 accumulation in rhabdomeres (Fig. 2E). These results indicate that the deficiencies of Rh1 transport and rhabdomere structure in PIG mutants are not a consequence of the loss of Chp function.

## Synthesis, transport and degradation of Rh1 in PIG-deficient photoreceptors

To identify the step of Rh1 synthesis or transport that is inhibited in PIG mutants, we clarified the dynamics of Rh1 transport using blue light-induced chromophore supply (BLICS) (Satoh et al., 1997; Satoh et al., 2005). Briefly, Rh1 comprises an apoprotein called opsin (also known as NinaE) and the chromophore 11-*cis* retinal. Without the chromophore, opsin accumulates in the ER. Blue-light illumination photoisomerizes retinal from all-*trans* to 11-*cis*, inducing the synchronous release of Rh1 from the ER into the secretory pathway.

Prior to BLICS, Rh1 apoprotein colocalized with ER markers (data not shown) in both wild-type and GPI-deficient photoreceptors (Fig. 3A,B, 0 minutes). Forty minutes after BLICS, Rh1 was concentrated in large dot-like structures, shown to be fly Golgi units, in both wild-type and GPI-deficient photoreceptors (Fig. 3A,B, 40 minutes). The colocalization of Rh1 with a Golgi marker confirmed the Golgi localization of Rh1 in GPI-deficient photoreceptors (Fig. 3C). These results indicate that Rh1 is normally synthesized and transported to Golgi units in GPI-deficient photoreceptors.

Sixty minutes after BLICS, Rh1 was not only concentrated in the Golgi units, but also localized at the base of the rhabdomeres, appearing as dot-like staining patterns in wild-type photoreceptors (Fig. 3A, 60 minutes). By contrast, in GPI-deficient photoreceptors, Rh1 was not localized at the base of the rhabdomeres but in irregular-shaped cytoplasmic organelles (Fig. 3B, 60 minutes) containing the endosomal markers Rab7 and Rbsn5 (Rbsn-5) (Tanaka and Nakamura, 2008) (Fig. 3E; data not shown). However, Rh1 and Rab7 or Rbsn5 did not colocalize in the wild-type cells (Fig. 3D; data not shown).

Rh1 transport was complete and Rh1 had strongly accumulated in the rhabdomeres in the wild-type cells by 180 minutes after

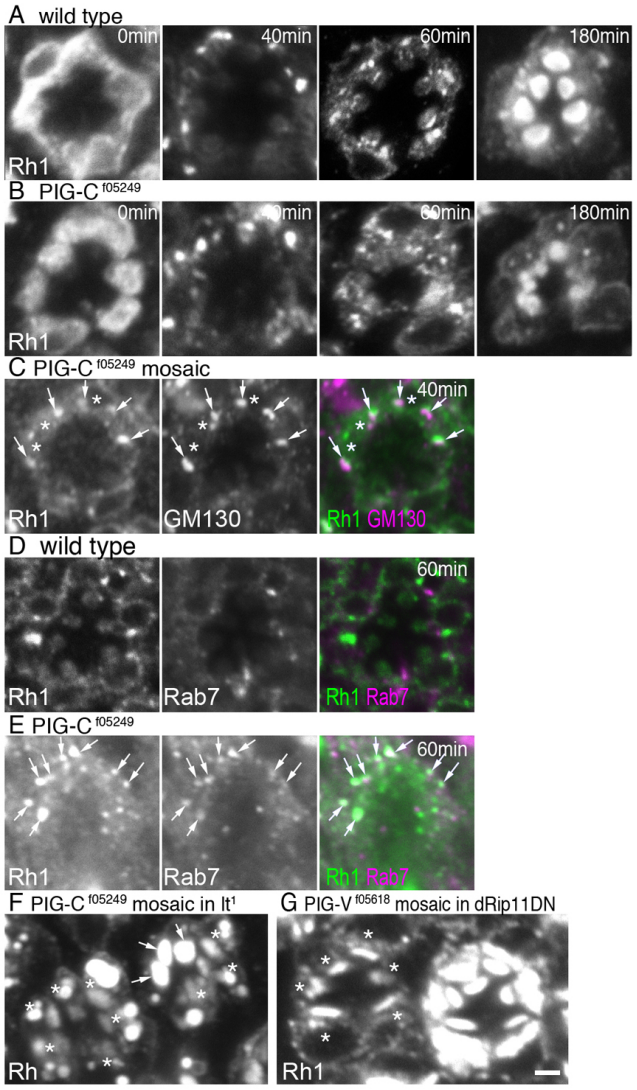


**Fig. 3. Kinetics of Rh1 transport.** (**A**,**B**) Immunostaining of Rh1 before and after BLICS in *Drosophila* wild-type (A) and *PIG-C*-mutant ommatidia (B). (**C**) Immunostaining of Rh1 (green) and Golgi marker, GM130 (magenta) 40 min after BLICS in *PIG-C*-mutant ommatidia. Asterisks show *PIG-C*–null photoreceptors. Arrows indicate Golgi units. (**D**,**E**) Immunostaining of Rh1 (green) and the endolysosome marker Rab7 (magenta) at 60 minutes after BLICS in wild-type (D) and *PIG-C*-mutant (E) ommatidia. Arrows show colocalization. (**F**) Projection image from five slices at 0.5-μm intervals of *PIG-C*-null mosaic eye with $lt^1$ homozygous background. Asterisks show *PIG-C*-null $lt^1$ double-mutant photoreceptors. $lt^1$ single-mutant photoreceptors and R4-R6 photoreceptors of the right-hand ommatidium accumulated Rh1 in the rhabdomeres; no cytoplasmic Rh1 staining is visible. Arrows indicate the rhabdomeres of wild-type photoreceptors. (**G**) *PIG-V*-null mosaic eye expressing Rip11 dominant-negative proteins by *Rh1Gal4* driver. Asterisks show *PIG-V*-null photoreceptors. Scale bars: 2 μm.

BLICS (Fig. 3A, 180 minutes). However, in GPI-deficient photoreceptors, only a limited amount of Rh1 reached the rhabdomeres. Interestingly, Rh1 was not observed in the cytoplasm in GPI-deficient photoreceptors (Fig. 3B, 180 minutes). These results indicate that most Rh1 is degraded within 180 minutes after Golgi arrival in GPI-deficient photoreceptors. The colocalization of Rh1 with the endosomal markers Rbsn5 and Rab7 60 minutes after BLICS suggests that Rh1 is degraded by the endolysosomal

system (Fig. 3E; data not shown). To investigate this possibility, we introduced an $lt^1$ homozygous viable mutation into PIG mosaic flies to inhibit lysosomal degradation. The *lt* gene encodes a homolog of yeast *Vps41p*, which is a component of the HOPS (homotypic vacuole fusion and protein sorting) complex. The degradation of endosomal cargo is inhibited in an $lt^1$ homozygous background (Chinchore et al., 2009). We observed more Rh1-positive staining in the cytoplasmic organelles in PIG-C/$lt^1$ double-mutant photoreceptors than in $lt^1$ or *PIG-C* single-mutant cells (Fig. 3F versus Fig. 1F). Therefore, Rh1 is degraded by the endolysosomal system in *PIG* null-mutant photoreceptors.

## Epistatic analysis between GPI synthesis and the Rab11-Rip11-MyoV complex

We previously showed that the Rab11-Rip11-MyoV complex is essential for post-Golgi vesicle transport and that a deficiency in any component of the complex induces the accumulation of Rh1-loaded post-Golgi vesicles in the cytoplasm (Satoh et al., 2005; Li et al., 2007). To investigate the epistatic interaction between the Rab11-Rip11-MyoV complex and GPI synthesis for Rh1 transport, we observed Rh1 localization in the *PIG-V* mutant mosaic retina expressing Rip11 dominant-negative protein. *Rip11-PIG-V* double-mutant photoreceptors did not accumulate Rh1 in the cytoplasm and the small amount of Rh1 localized in the rhabdomeres (Fig. 3G). This phenotype was indistinguishable from that of cells with only a *PIG-V* mutation (Fig. 1G). This result indicates that GPI synthesis is epistatic to the Rab11-Rip11-MyoV complex. Kinetic and epistatic analyses of Rh1 transport in GPI-deficient cells revealed that GPI synthesis is necessary for processes after Golgi entry and before/upon post-Golgi vesicle formation during Rh1 biosynthetic trafficking.

## Mislocalization of $Na^+K^+$-ATPase and Crb to the rhabdomeres in GPI-deficient photoreceptors

In addition to their Rh1 transport deficiency, PIG mutants show another remarkable transport phenotype. Unlike other mutants identified in our screening (supplementary material Table S1), PIG mutants show rhabdomeric mistargeting of a basolateral membrane protein, $Na^+K^+$-ATPase, and a stalk membrane protein, Crb. In wild-type 90% pupal development (pd) and older R1-R6 photoreceptors, $Na^+K^+$-ATPase localized only on the basolateral membrane. In GPI-deficient cells, significant amounts of $Na^+K^+$-ATPase were detected in the rhabdomere, whereas less $Na^+K^+$-ATPase was present on the basolateral membrane (Fig. 4A; supplementary material Fig. S3A-D). Crb specifically localized to the stalk membrane in wild-type photoreceptors; however, in GPI-deficient cells, Crb also localized to the rhabdomeres (Fig. 4B; data not shown). These results indicate that GPI deficiency induces the mislocalization of basolateral and stalk membrane proteins to the rhabdomere membrane. However, this mislocalization was not caused by defects in adherens junction formation, because adherens junctions formed normally (Fig. 2B, arrowheads) and a component of adherens junctions, DE-cadherin (Shotgun – FlyBase), exhibited normal localization in PIG-deficient ommatidia (Fig. 4C). Moreover, although continuous photoreceptor adherens junctions are not formed in a *Crb* mutant, $crb^{11A22}$ (Pellikka et al., 2002), Rh1 and $Na^+K^+$-ATPase localized normally on the rhabdomeres and basolateral membrane, respectively (Fig. 4D; supplementary material Movies 1, 2). These results indicate that the defects of Rh1 transport and $Na^+K^+$ATPase mislocalization in rhabdomeres in PIG mutants are not caused by disruption of the continuity of the adherens junctions.

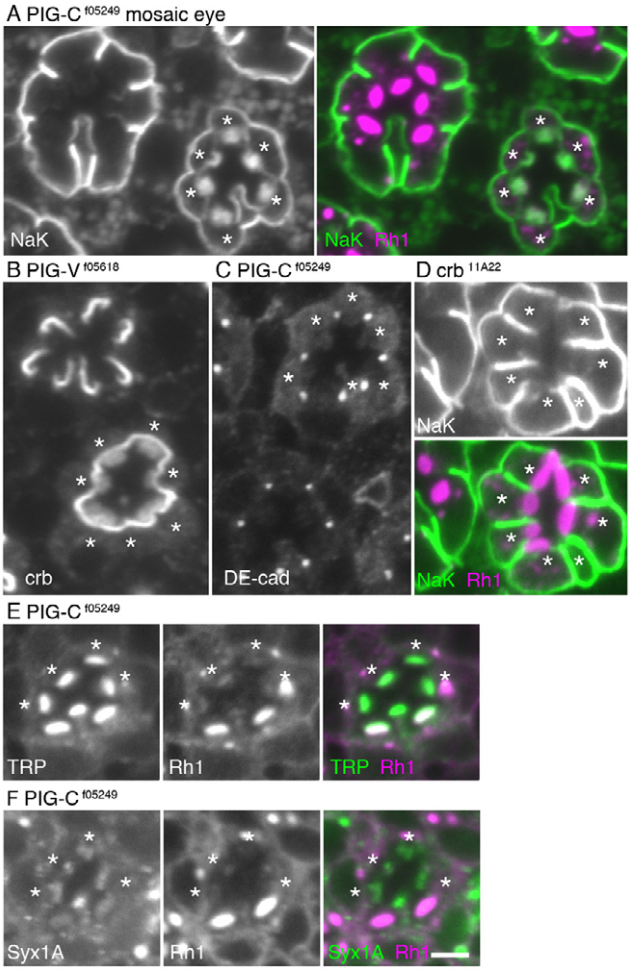


**Fig. 4. Mislocalization of $Na^+K^+$-ATPase and Crb to the rhabdomeres in GPI-deficient photoreceptors.** Immunostaining of *Drosophila* mosaic retina containing both wild-type and mutant photoreceptors. Asterisks show mutant photoreceptors. Mutant alleles and antibodies used are specified below. (**A**) *PIG-C* $^{f05249}$ mosaic retina. $Na^+K^+$-ATPase (green) and Rh1 (magenta). (**B**) *PIG-V* $^{f05618}$ mosaic retina. Crb staining. (**C**) *PIG-C* $^{f05249}$ mosaic retina. DE-cadherin (DE-cad) staining. (**D**) $crb^{11A22}$ mosaic retina. $Na^+K^+$-ATPase (green) and Rh1 (magenta). The stalk membrane in $crb^{11A22}$ mutant photoreceptor is short, as shown by Pellikka et al. (Pellikka et al. 2002). (**E**) *PIG-C* $^{f05249}$ mosaic retina. TRP (green) and Rh1 (magenta). (**F**) *PIG-C* $^{f05249}$ mosaic retina. Syx1A (green) and Rh1 (magenta). Scale bars: 2 μm.

Therefore, the defects in adherens junction formation do not explain the Rh1 transport deficiency or $Na^+K^+$-ATPase mislocalization in PIG mutants. Taken together, the mislocalizations of $Na^+K^+$-ATPase and Crb and deficiency in Rh1 transport indicate that the sorting machinery at the TGN concentrates Rh1 into post-Golgi vesicles destined for the rhabdomeres while excluding $Na^+K^+$-ATPase and Crb, and that this process requires GPI synthesis.

## Exclusion mechanism of rhabdomere-directed transport vesicles

The hypothesis that a lack of exclusion from post-Golgi vesicle precursors at the TGN in PIG mutants causes the mislocalization of $Na^+K^+$-ATPase is supported by the phenotype of the mutants of AP1γ and AP47, which are components of the AP-1 complex

involved in the recruitment of basolateral proteins in the TGN (Fölsch et al., 1999; Gonzalez and Rodriguez-Boulan, 2009; Benhra et al., 2011). In *AP1γ*$^{e454e6}$ and *AP47*$^{GS15243}$ mutants, $Na^+K^+$-ATPase was mistransported to the apical stalk membrane but not to the rhabdomeres (supplementary material Fig. S3E; data not shown). This mis-sorting phenotype of AP-1 mutants indicates that overloaded $Na^+K^+$-ATPase in the TGN can be misloaded into vesicles destined for the stalk membrane when it fails to be recruited into basolateral transport vesicles. Moreover, the fact that $Na^+K^+$-ATPase is still excluded from the rhabdomere even in the *AP1* mutants suggests that rhabdomere-directed transport vesicles have a strict exclusion mechanism that excludes proteins with other destinations and that GPI-deficient cells lack this essential exclusion mechanism.

Next, we investigated the localization of other rhabdomeric transmembrane proteins including TRP and syntaxin 1A (Syx1A). In contrast to Rh1, the localizations of TRP and Syx1A were not substantially reduced in PIG mutants; near normal levels of TRP and Syx1A localized to the rhabdomeres (Fig. 4E,F). Thus, not all rhabdomeric proteins require GPI synthesis to be delivered to the rhabdomere.

## Rh1 transport defects and $Na^+K^+$-ATPase mislocalization in earlier developmental stages and partially rescued flies

A recent paper reports a similar Rh1 reduction in *PIG-V* hypomorphic mutant photoreceptors and explains that it is a secondary defect caused by the disruption of rhabdomeres by Chp deficiency (Rosenbaum et al., 2012). However, in our studies, the near-normal localizations of TRP and Syx1A in the rhabdomeres of null mutants and the BLICS analysis provide evidence that the Rh1 transport defect is not caused by the secondary defect. To rule out the possibility that the secondary defect causes Rh1 and $Na^+K^+$-ATPase transport defects, we performed two kinds of observations. First, we examined the earlier stages of eye development. Before 73% pd, Rh1 transport was already clearly defective and much $Na^+K^+$-ATPase had mislocalized in the rhabdomeres (Fig. 5B). The mislocalization of $Na^+K^+$-ATPase was clear even at 55% pd (Fig. 5A); however, we could not investigate Rh1 transport deficiency at this time point, because Rh1 expression starts at around 70% pd. Electron microscope observations revealed that rhabdomere structure profiles were much better at 58% and 73% pd than at the late-pupal stage (i.e. 80-100% pd) and that TRP accumulated normally in the rhabdomeres at both time points (Fig. 5A,C). Second, we examined late-pupal retinas (>80% pd) of partially rescued *PIG-C* mosaic retinas that expressed the *PIG-C* gene via *eyeless-Gal4*. Because *eyeless-Gal4* induces *PIG-C* gene expression at an early stage of eye development but stops this induction before the mid-pupal stage, we can analyze the effect of *PIG-C* deficiency while avoiding its effect in early eye development. We still observed the PIG phenotype (i.e. Rh1 transport defect, $Na^+K^+$-ATPase mislocalization and Chp accumulation in the ER) on these partially rescued *PIG-C* mosaic retinas (supplementary material Fig. S4A,B). Electron microscopic observations showed that the rhabdomeres were small but their microvilli showed better shapes (supplementary material Fig. S4C). Both results strongly support our hypothesis that *PIG* genes are essential for Rh1 transport to and $Na^+K^+$ATPase exclusion from the rhabdomeres.

## Sorting of Rh1 in the TGN and lipid raft model

In polarized epithelial cells, most GPI-anchored proteins are transported to the apical membrane and associate with detergent-resistant membrane (DRM). Lipid rafts, which are normally isolated as DRM, are believed to play an important role in protein sorting at the TGN or the recycling endosomes of polarized epithelial cells (Rodriguez-Boulan et al., 2005). The lipid raft hypothesis states that lipid rafts, which are microdomains rich in glycosphingolipids and cholesterol, concentrate some fractions of apically destined proteins by their affinity (van Meer and Simons, 1988). Therefore, we investigated the lipid raft deficiency in PIG mutants and the association between DRM and Rh1. The rhabdomere is a cholesterol-rich membrane domain (Fig. 6A) (Sanxaridis et al., 2007). In GPI-deficient photoreceptors, cholesterol was less concentrated in the rhabdomeres (Fig. 6A) and diffused more in the basolateral membrane. This result suggests that raft formation in photoreceptors is affected in PIG mutants. However, the reduced filipin staining in the rhabdomeres of PIG mutants could be the result of the less-condensed rhabdomere membrane. At least part of rhabdomeric membrane can be isolated

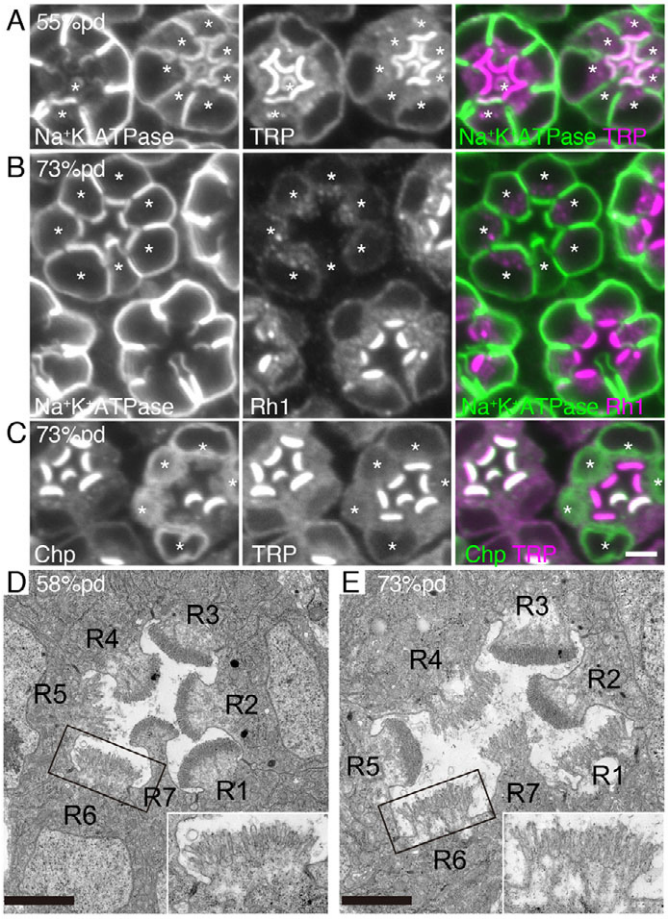


**Fig. 5. Deficiencies of Rh1 and $Na^+K^+$-ATPase transport in earlier developmental stages.** (**A-C**) Immunostaining of *Drosophila* mosaic retina containing both wild-type and *PIG-C*$^{f05249}$ photoreceptors. Asterisks show mutant photoreceptors. Developmental stages and antibodies used are specified below: (A) 55% pd retina stained by $Na^+K^+$-ATPase (green) and TRP (magenta). (B) 73% pd retina stained by $Na^+K^+$-ATPase (green) and Rh1 (magenta). (C) 73% pd retina stained by Chp (green) and TRP (magenta). (**D**,**E**) Observation of *PIG-C*$^{f05249}$ mosaic ommatidium at 58% (D) and 73% (E) by electron microscopy. R5 and R6 photoreceptors in D and R1, R4, R6 and R7 photoreceptors in E are *PIG-C*-null mutants. Insets are high-magnification images of R6 rhabdomeres. Scale bars: 2 μm.

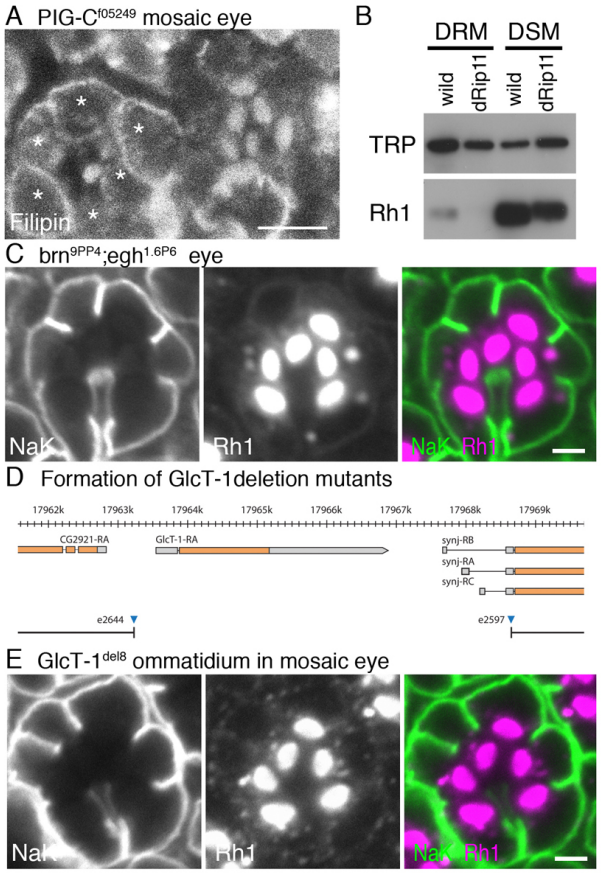


**Fig. 6. Lipid raft-independent sorting of Rh1 at the TGN.** (**A**) Filipin staining in *Drosophila* mosaic retina containing both wild-type and *PIG-C*-null mutant photoreceptors. Asterisks show *PIG-C* mutant cells. Scale bar: 5 μm. (**B**) Immunoblot analysis of the associations of TRP and Rh1 with DRM in wild-type and dominant-negative *Rip11*-expressing retina. Membranes of homogenates from illuminated wild-type heads (lanes 1 and 3) and illuminated *Rip11DN/ Rh1Gal4* heads (lanes 2 and 4) were separated into DRMs and detergent-soluble membranes (DSMs). (**C**) Immunostaining of $Na^+K^+$-ATPase (green) and Rh1 (magenta) in $brn^{9PP4}$, $egh^{1.6P6}$ double-mutant ommatidium. Scale bar: 2 μm. (**D**) Formation of *GlcT-1* deletion mutants. Two transposon insertion lines, $GlcT\text{-}1^{e2644}$ and $GlcT\text{-}1^{e2597}$, containing the *FRT* sequence were used to make *GlcT-1* deletion mutants using the *FLP/FRT* method. $GlcT\text{-}1^{\Delta 8}$ includes a part of *synaptojanin* in addition to *GlcT-1*. (**E**) Immunostaining of a cross section of a $GlucT\text{-}1^{\Delta 8}$ ommatidium. Rh1 (magenta) and $Na^+K^+$-ATPase (green). Scale bar: 2 μm.

as DRM in fly photoreceptors, and a rhabdomeric protein, TRP, associates with DRM in a light-dependent manner whereas mature Rh1 does not (Sanxaridis et al., 2007). We first confirmed that TRP associates with DRM isolated from light-exposed wild-type heads and that Rh1 does not (Fig. 6B). Next, we tested whether newly synthesized Rh1 can be temporally associated with DRM in the post-Golgi vesicles. To obtain DRM from the post-Golgi vesicles, we isolated DRM from *Rip11* mutant whole eyes (data not shown) and retinas expressing Rip11 dominant-negative protein, which accumulate post-Golgi vesicles carrying Rh1 in the cytoplasm. The results show that Rh1 did not associate with DRM in these mutants despite the strong association between TRP and DRM (Fig. 6B).

Next, we investigated whether the sorting phenotype can be observed in a mutant lacking glycosphingolipids, an essential raft component. *brainiac* (*brn*) encodes a UDP-*N*-acetylglucosamine, βMan β1,3-*N*-acetylglucosaminyltransferase (β3GlcNAc-transferase), and *egghead* (*egh*) encodes a GDP-mannose, βGlc β1,4-mannosyltransferase, with putative functions in sequential steps in the biosynthesis of the core structure of arthro-series glycosphingolipids (GlcNAcβ1–3Manβ1–4Glcβ1-Cer). It is reported that $brn^{9PP4}/egh^{1.6P6}$ double mutants lack glycosphingolipids and accumulate monoglucosylated ceramide (Wandall et al., 2005). Rh1 and $Na^+K^+$-ATPase localized normally in the rhabdomeres and basolateral membrane, respectively, in $brn^{9PP4}/egh^{1.6P6}$ double-mutant photoreceptors (Fig. 6C). We also investigated the deletion mutants of the sole fly ceramide glucosyltransferase, *GlcT-1*, which is the first step of glycosphingolipid synthesis; the product itself was recently shown to play an essential role in apical sorting in nematodes (Zhang et al., 2011). The homozygous *GlcT-1* mutant photoreceptors in the mosaic retina exhibited normal morphology and Rh1 and $Na^+K^+$-ATPase localization (Fig. 6D,E), indicating that the sorting defects observed in the PIG mutants are not due to the possible glucosyl ceramide reduction. In addition, Rh1 expression in cholesterol-deficient flies is not drastically reduced (Sanxaridis et al., 2007). These results collectively indicate Rh1 and $Na^+K^+$-ATPase sorting at the TGN in fly photoreceptors is not strongly affected by lipid raft deficiency.

## DISCUSSION

In this study, we screened 546 lethal lines for potential defects in Rh1 by examining the localization of Arr2::GFP in *FLP/FRT*-mediated mosaic retinas using two-color fluorescence imaging. We found a mutation in the *Drosophila* homolog of human *PIG-U*, which encodes a subunit of GPI transamidase. Mutations in other genes of the GPI synthesis pathway but not in the GPI modification pathway gave rise to the same phenotype. Furthermore, the GPI-linked protein, Chp accumulates in the ER whereas the stalk membrane Crumbs protein and basolaterally localized $Na^+K^+$-ATPase were mis-sorted to the rhabdomere. We demonstrated that Rh1 is degraded before entering the post-Golgi vesicles but that Crb and $Na^+K^+$-ATPase are misrouted into vesicles destined for the rhabdomere in PIG mutant cells.

There are two reports concerning GPI requirements for the transport of transmembrane proteins. In zebrafish, GPI transamidase is essential for the surface expression of voltage-gated sodium channels (Nakano et al., 2010). In yeast, GPI synthesis is required for the surface expression of Tat2p tryptophan permease, which is associated with DRM in wild-type cells. In GPI-deficient yeast, Tat2p and Fur4p fail to associate with DRM and are retained in the ER (Okamoto et al., 2006). Although DRM forms in the ER in yeast, in mammalian cells, it is likely that DRM formation occurs only after Golgi entry (Rivier et al., 2010). The reason for this is thought to be that GPI lipid remodeling occurs in different places: the ER in yeast and the Golgi body in mammalian cells (Rivier et al., 2010). In mammalian cells, lipid rafts are postulated to concentrate some fractions of apically destined proteins owing to their affinity for the TGN (van Meer and Simons, 1988) or recycling endosomes (Rodriguez-Boulan et al., 2005).

Along with the raft model, there are two possible explanations for the sorting phenotype of PIG mutant fly photoreceptors: (1) the polarized sorting of Rh1 depends on its affinity for the raft/DRM and the raft/DRM is deficient in PIG mutants; (2) unidentified GPI-anchored protein(s) play crucial roles in the polarized sorting of Rh1 and $Na^+K^+$-ATPase, and the raft/DRM provides a platform for the GPI-anchored protein(s). The first model predicts raft/DRM deficiency in PIG mutants, Rh1 association with lipid rafts and a stronger phenotype caused by mutations in the genes involved in

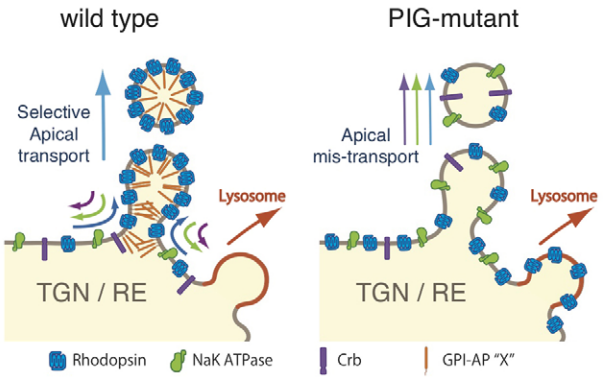


**Fig. 7. Model of protein sorting at the TGN.** In the wild-type TGN, one or more GPI-anchored protein localizes to the neck and/or inside budding post-Golgi vesicles destined for the rhabdomeres and recruits rhabdomere proteins but excludes others. By contrast, GPI-deficient TGNs do not contain GPI-anchored proteins and do not perform protein sorting. Consequently, most Rh1 is sent to the endocytotic pathway and degraded by lysosomes whereas small amounts of Rh1, $Na^+K^+$-ATPase and Crb are loaded into post-Golgi vesicles for delivery to the rhabdomeres.

raft formation. By contrast, the second model predicts that GPI deficiency produces a stronger phenotype than that caused by raft deficiency.

Our analysis of lipid raft deficiency (Fig. 6) does not support the first model in which the loss of polarized sorting of Rh1/$Na^+K^+$-ATPase in PIG mutants is a consequence of raft deficiency; instead, our results support the second model in which unidentified GPI-anchored protein(s) concentrate Rh1 and exclude $Na^+K^+$-ATPase and Crb from post-Golgi vesicles destined for the rhabdomeres. Thus, loss of the GPI-anchored sorting protein(s) might cause most Rh1 to be directed into the endocytotic pathway and degraded by lysosomes while simultaneously allowing $Na^+K^+$-ATPase and Crb to be loaded into post-Golgi vesicles destined for the rhabdomeres (Fig. 7). Chp is the only GPI-anchored protein known to be expressed in fly photoreceptors in the late-pupal stages (Reinke et al., 1988). However, *chp*$^2$ mutants do not exhibit any mislocalization phenotype of Rh1 or $Na^+K^+$-ATPase (Fig. 2E; supplementary material Fig. S3F). Identifying the GPI-anchored protein(s) responsible for the sorting in the TGN is an important step for understanding this mechanism of polarized transport.

The biosynthetic pathway of GPI-anchored proteins has been well elucidated, but little was known to date about the phenotypic consequences of the loss of GPI synthesis *in vivo*. The present study demonstrates that GPI synthesis is essential for the sorting of non-GPI-anchored transmembrane proteins, including Rh1 and $Na^+K^+$-ATPase, without obvious defects in adherens junctions. Human PIGM or PIGV deficiency causes seizures (Almeida et al., 2006) or mental retardation (Krawitz et al., 2010). These neurological disorders might be also caused by the mis-sorting of some transmembrane proteins in addition to the defects in the formation of GPI-anchoring proteins. Our findings aid the understanding of the pathology of diseases involving deficient GPI-anchoring protein synthesis.

**Acknowledgements**
We thank Drs A. Nakamura, U. Tepass, C. Montell and C. Zuker, who kindly provided fly stocks and reagents. We also thank the Bloomington Stock Center and the *Drosophila* Genetic Resource Center of the Kyoto Institute of Technology for fly stocks.

**Funding**
This study was supported by the Naito Foundation [25-040920]; the Novartis Foundation [25-050421]; the Hayashi Memorial Foundation for Female Natural Scientists [25-051022]; PRESTO [25-J-J4215]; KAKENHI [21687005, 21113510 and 23113712 to A.S.K.]; and the Swiss National Science Foundation professorship [to R.W.]. This study was also supported by the Global Centers of Excellence Program 'Advanced Systems-Biology: Designing The Biological Function' from the Japanese Ministry of Education, Culture, Sports, Science, and Technology.

**Competing interests statement**
The authors declare no competing financial interests.

**Supplementary material**
Supplementary material available online at
http://dev.biologists.org/lookup/suppl/doi:10.1242/dev.083683/-/DC1

**References**

**Adam, R. M., Yang, W., Di Vizio, D., Mukhopadhyay, N. K. and Steen, H.** (2008). Rapid preparation of nuclei-depleted detergent-resistant membrane fractions suitable for proteomics analysis. *BMC Cell Biol.* **9**, 30.
**Almeida, A. M., Murakami, Y., Layton, D. M., Hillmen, P., Sellick, G. S., Maeda, Y., Richards, S., Patterson, S., Kotsianidis, I., Mollica, L. et al.** (2006). Hypomorphic promoter mutation in PIGM causes inherited glycosylphosphatidylinositol deficiency. *Nat. Med.* **12**, 846-851.
**Benhra, N., Lallet, S., Cotton, M., Le Bras, S., Dussert, A. and Le Borgne, R.** (2011). AP-1 controls the trafficking of Notch and Sanpodo toward E-cadherin junctions in sensory organ precursors. *Curr. Biol.* **21**, 87-95.
**Beronja, S., Laprise, P., Papoulas, O., Pellikka, M., Sisson, J. and Tepass, U.** (2005). Essential function of Drosophila Sec6 in apical exocytosis of epithelial photoreceptor cells. *J. Cell Biol.* **169**, 635-646.
**Bischof, J., Maeda, R. K., Hediger, M., Karch, F. and Basler, K.** (2007). An optimized transgenesis system for Drosophila using germ-line-specific phiC31 integrases. *Proc. Natl. Acad. Sci. USA* **104**, 3312-3317.
**Chen, J., Call, G. B., Beyer, E., Bui, C., Cespedes, A., Chan, A., Chan, J., Chan, S., Chhabra, A., Dang, P. et al.** (2005). Discovery-based science education: functional genomic dissection in Drosophila by undergraduate researchers. *PLoS Biol.* **3**, e59.
**Chinchore, Y., Mitra, A. and Dolph, P. J.** (2009). Accumulation of rhodopsin in late endosomes triggers photoreceptor cell degeneration. *PLoS Genet.* **5**, e1000377.
**Colley, N. J., Baker, E. K., Stamnes, M. A. and Zuker, C. S.** (1991). The cyclophilin homolog ninaA is required in the secretory pathway. *Cell* **67**, 255-263.
**Fölsch, H., Ohno, H., Bonifacino, J. S. and Mellman, I.** (1999). A novel clathrin adaptor complex mediates basolateral targeting in polarized epithelial cells. *Cell* **99**, 189-198.
**Fujita, M. and Kinoshita, T.** (2010). Structural remodeling of GPI anchors during biosynthesis and after attachment to proteins. *FEBS Lett.* **584**, 1670-1677.
**Gambis, A., Dourlen, P., Steller, H. and Mollereau, B.** (2011). Two-color *in vivo* imaging of photoreceptor apoptosis and development in Drosophila. *Dev. Biol.* **351**, 128-134.
**Gonzalez, A. and Rodriguez-Boulan, E.** (2009). Clathrin and AP1B: key roles in basolateral trafficking through trans-endosomal routes. *FEBS Lett.* **583**, 3784-3795.
**Izaddoost, S., Nam, S. C., Bhat, M. A., Bellen, H. J. and Choi, K. W.** (2002). Drosophila Crumbs is a positional cue in photoreceptor adherens junctions and rhabdomeres. *Nature* **416**, 178-183.
**Krantz, D. E. and Zipursky, S. L.** (1990). Drosophila chaoptin, a member of the leucine-rich repeat family, is a photoreceptor cell-specific adhesion molecule. *EMBO J.* **9**, 1969-1977.
**Krawitz, P. M., Schweiger, M. R., Rödelsperger, C., Marcelis, C., Kölsch, U., Meisel, C., Stephani, F., Kinoshita, T., Murakami, Y., Bauer, S. et al.** (2010). Identity-by-descent filtering of exome sequence data identifies PIGV mutations in hyperphosphatasia mental retardation syndrome. *Nat. Genet.* **42**, 827-829.
**Kumar, J. P. and Ready, D. F.** (1995). Rhodopsin plays an essential structural role in Drosophila photoreceptor development. *Development* **121**, 4359-4370.
**Li, B. X., Satoh, A. K. and Ready, D. F.** (2007). Myosin V, Rab11, and dRip11 direct apical secretion and cellular morphogenesis in developing Drosophila photoreceptors. *J. Cell Biol.* **177**, 659-669.
**Maeda, Y. and Kinoshita, T.** (2011). Structural remodeling, trafficking and functions of glycosylphosphatidylinositol-anchored proteins. *Prog. Lipid Res.* **50**, 411-424.
**Mollereau, B., Wernet, M. F., Beaufils, P., Killian, D., Pichaud, F., Kühnlein, R. and Desplan, C.** (2000). A green fluorescent protein enhancer trap screen in Drosophila photoreceptor cells. *Mech. Dev.* **93**, 151-160.

**Murakami, Y., Kanzawa, N., Saito, K., Krawitz, P. M., Mundlos, S., Robinson, P. N., Karadimitris, A., Maeda, Y. and Kinoshita, T.** (2012). Mechanism for release of alkaline phosphatase caused by glycosylphosphatidylinositol deficiency in patients with hyperphosphatasia mental retardation syndrome. *J. Biol. Chem.* **287**, 6318-6325.
**Nakano, Y., Fujita, M., Ogino, K., Saint-Amant, L., Kinoshita, T., Oda, Y. and Hirata, H.** (2010). Biogenesis of GPI-anchored proteins is essential for surface expression of sodium channels in zebrafish Rohon-Beard neurons to respond to mechanosensory stimulation. *Development* **137**, 1689-1698.
**Nozaki, M., Ohishi, K., Yamada, N., Kinoshita, T., Nagy, A. and Takeda, J.** (1999). Developmental abnormalities of glycosylphosphatidylinositol-anchor-deficient embryos revealed by Cre/loxP system. *Lab. Invest.* **79**, 293-299.
**Okamoto, M., Yoko-o, T., Umemura, M., Nakayama, K. and Jigami, Y.** (2006). Glycosylphosphatidylinositol-anchored proteins are required for the transport of detergent-resistant microdomain-associated membrane proteins Tat2p and Fur4p. *J. Biol. Chem.* **281**, 4013-4023.
**Ozaki, K., Nagatani, H., Ozaki, M. and Tokunaga, F.** (1993). Maturation of major Drosophila rhodopsin, ninaE, requires chromophore 3-hydroxyretinal. *Neuron* **10**, 1113-1119.
**Parks, A. L., Cook, K. R., Belvin, M., Dompe, N. A., Fawcett, R., Huppert, K., Tan, L. R., Winter, C. G., Bogart, K. P., Deal, J. E. et al.** (2004). Systematic generation of high-resolution deletion coverage of the Drosophila melanogaster genome. *Nat. Genet.* **36**, 288-292.
**Pellikka, M., Tanentzapf, G., Pinto, M., Smith, C., McGlade, C. J., Ready, D. F. and Tepass, U.** (2002). Crumbs, the Drosophila homologue of human CRB1/RP12, is essential for photoreceptor morphogenesis. *Nature* **416**, 143-149.
**Pichaud, F. and Desplan, C.** (2001). A new visualization approach for identifying mutations that affect differentiation and organization of the Drosophila ommatidia. *Development* **128**, 815-826.
**Reinke, R., Krantz, D. E., Yen, D. and Zipursky, S. L.** (1988). Chaoptin, a cell surface glycoprotein required for Drosophila photoreceptor cell morphogenesis, contains a repeat motif found in yeast and human. *Cell* **52**, 291-301.
**Rivier, A. S., Castillon, G. A., Michon, L., Fukasawa, M., Romanova-Michaelides, M., Jaensch, N., Hanada, K. and Watanabe, R.** (2010). Exit of GPI-anchored proteins from the ER differs in yeast and mammalian cells. *Traffic* **11**, 1017-1033.
**Rodriguez-Boulan, E., Kreitzer, G. and Müsch, A.** (2005). Organization of vesicular trafficking in epithelia. *Nat. Rev. Mol. Cell Biol.* **6**, 233-247.
**Rosenbaum, E. E., Brehm, K. S., Vasiljevic, E., Gajeski, A. and Colley, N. J.** (2012). Drosophila GPI-mannosyltransferase 2 is required for GPI anchor attachment and surface expression of chaoptin. *Vis. Neurosci.* **29**, 143-156.
**Sanxaridis, P. D., Cronin, M. A., Rawat, S. S., Waro, G., Acharya, U. and Tsunoda, S.** (2007). Light-induced recruitment of INAD-signaling complexes to detergent-resistant lipid rafts in Drosophila photoreceptors. *Mol. Cell. Neurosci.* **36**, 36-46.
**Satoh, A. and Ready, D.** (2005). Arrestin1 mediates light-dependent rhodopsin endocytosis and cell survival. *Curr. Biol.* **15**, 1722-1733.
**Satoh, A. K., Tokunaga, F., Kawamura, S. and Ozaki, K.** (1997). *In situ* inhibition of vesicle transport and protein processing in the dominant negative Rab1 mutant of Drosophila. *J. Cell Sci.* **110**, 2943-2953.
**Satoh, A. K., O'Tousa, J. E., Ozaki, K. and Ready, D. F.** (2005). Rab11 mediates post-Golgi trafficking of rhodopsin to the photosensitive apical membrane of Drosophila photoreceptors. *Development* **132**, 1487-1497.
**Satoh, A. K., Xia, H. A., Yan, L. M., Liu, C. H., Hardie, R. C. and Ready, D. F.** (2010). Arrestin translocation is stoichiometric to rhodopsin isomerization and accelerated by phototransduction in Drosophila photoreceptors. *Neuron* **67**, 997-1008.
**Shetty, K. M., Kurada, P. and O'Tousa, J. E.** (1998). Rab6 regulation of rhodopsin transport in Drosophila. *J. Biol. Chem.* **273**, 20425-20430.
**Takeda, J., Miyata, T., Kawagoe, K., Iida, Y., Endo, Y., Fujita, T., Takahashi, M., Kitani, T. and Kinoshita, T.** (1993). Deficiency of the GPI anchor caused by a somatic mutation of the PIG-A gene in paroxysmal nocturnal hemoglobinuria. *Cell* **73**, 703-711.
**Tanaka, T. and Nakamura, A.** (2008). The endocytic pathway acts downstream of Oskar in Drosophila germ plasm assembly. *Development* **135**, 1107-1117.
**van Meer, G. and Simons, K.** (1988). Lipid polarity and sorting in epithelial cells. *J. Cell. Biochem.* **36**, 51-58.
**Wandall, H. H., Pizette, S., Pedersen, J. W., Eichert, H., Levery, S. B., Mandel, U., Cohen, S. M. and Clausen, H.** (2005). Egghead and brainiac are essential for glycosphingolipid biosynthesis *in vivo*. *J. Biol. Chem.* **280**, 4858-4863.
**Xu, T. and Rubin, G. M.** (1993). Analysis of genetic mosaics in developing and adult Drosophila tissues. *Development* **117**, 1223-1237.
**Yasuhara, J. C., Baumann, O. and Takeyasu, K.** (2000). Localization of Na/K-ATPase in developing and adult *Drosophila melanogaster* photoreceptors. *Cell Tissue Res.* **300**, 239-249.
**Zhang, H., Abraham, N., Khan, L. A., Hall, D. H., Fleming, J. T. and Göbel, V.** (2011). Apicobasal domain identities of expanding tubular membranes depend on glycosphingolipid biosynthesis. *Nat. Cell Biol.* **13**, 1189-1201.

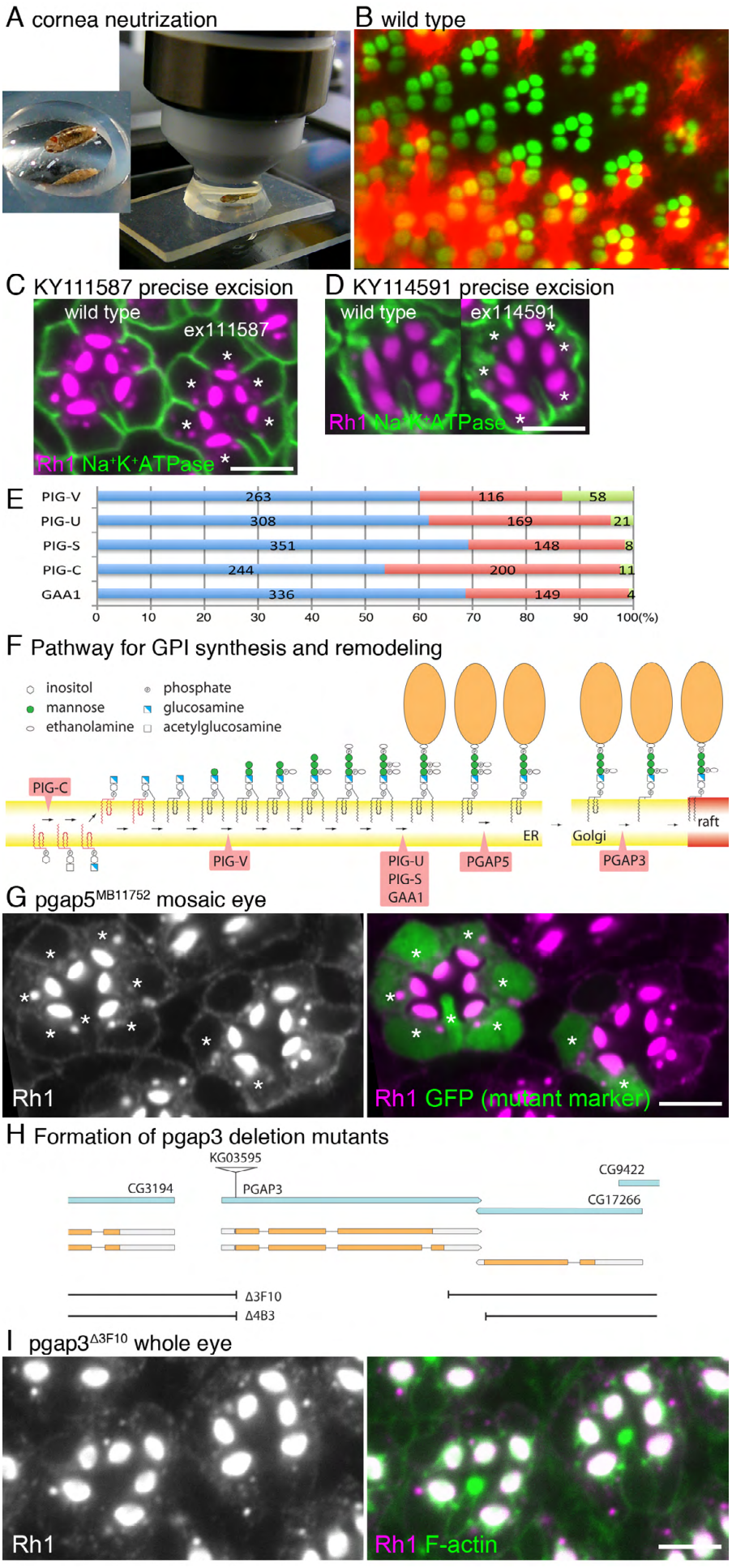


**Fig. S1. Inhibition of Rh1 accumulation on the rhabdomere membrane in *CG13089 PIG-U* mutants.** (**A**) Late pupae with dark wings were put into 0.2% agar after the pupal case was partially removed. Two fluorescent proteins expressed in photoreceptors were directly observed by confocal microscopy with a 40× water-immersion lens (i.e. cornea neutralization technique). RFP is only expressed in wild-type photoreceptors. Arrestin2::GFP is expressed in all R1-R6 peripheral photoreceptors. Arrestin2::GFP specifically exhibits endogenous Rh1 localization because of its high affinity for activated Rh1 formed after 470-nm illumination for GFP detection. It was more sensitive than Rh1-GFP fusion protein, which did not show rhabdomere localization at 80-90% pd (data not shown), suggesting a slower exit rate from the ER than endogenous Rh1. (**B**) Image obtained by observation of a mosaic retina using the cornea neutralization technique. In this retina, both RFP-positive and RFP-negative cells are wild type. (**C**,**D**) Immunostaining of the cross sections of mosaic eyes composed of wild-type cells (left ommatidium) and homozygous cells in which P-elements were precisely removed from the original KY111487 and KY114591 stock lines (right ommatidium). Rh1 (magenta) and $Na^+K^+$-ATPase (green) are transported to and accumulate in the rhabdomeres and basolateral membrane normally. Asterisks show mutant photoreceptors. Scale bar: 5 μm. (**E**) Proportions of wild-type and mutant ommatidia in *PIG*-mosaic retina. Confocal micrographs were obtained from ten individual mutant mosaic retina of homozygous *PIG*-mutant and RFP-expressing wild-type cells. Arr2-GFP and RFP were used to distinguish mutants from wild-type R1-R6 cells. Ommatidia consisting of R1-R6 photoreceptors of only wild-type (blue), only mutant (green), and both wild-type and mutant (red) cells were counted (numbers shown in the graph). (**F**) Schematic view of the biosynthetic and remodeling pathways of GPI-anchored proteins [modified with permission from Fig. 2 in the review by Fujita and Kinoshita (Fujita and Kinoshita, 2010)]. (**G**) Immunostaining of the cross section of $PGAP5^{MB11752}$ mosaic retina. Rh1 (magenta) was transported to and accumulated in the rhabdomeres normally. GFP is a mutant cell marker. (**H**) Generation of pgap3 deletion mutants by imprecise excision. The extent of deletions in $PGAP^{\Delta 4B3}$ and $PGAP3^{\Delta 3F10}$ induced by the imprecise excision of the KG03595 element alleles, which are mapped between *PGAP3* and CG3194. $PGAP3^{\Delta 3F10}$ does not contain the entire *PGAP3* gene, but other genes are intact. $PGAP3^{\Delta 4B3}$ may include part of *CG17266* in addition to *PGAP3*. Both *PGAP3* deletion mutants are viable. (**I**) Immunostaining of the cross section of $PGAP3^{\Delta 3F10}$ retina. Rh1 (magenta) was transported to and accumulated in the rhabdomeres normally. Scale bar: 5 μm.

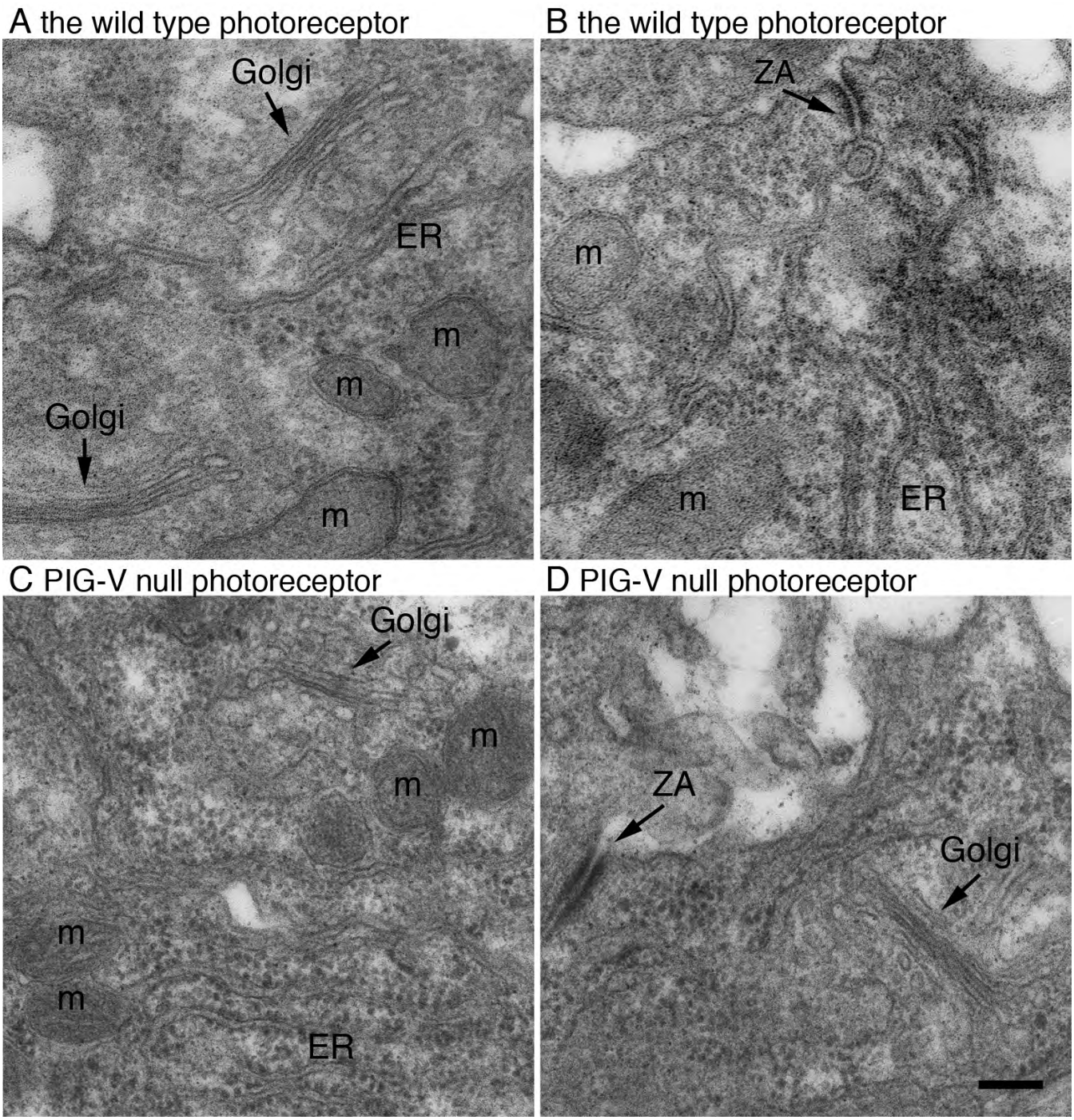


**Fig. S2. Electron microscopy of PIG-V photoreceptors.** Electron micrographs of wild-type (**A**,**B**) and *PIG-V*-null photoreceptors (**C**,**D**). ER, Golgi, zonula adherens junctions (ZA) and mitochondria (m) show normal appearance in *PIG-V*-null photoreceptors. Scale bar: 500 nm.

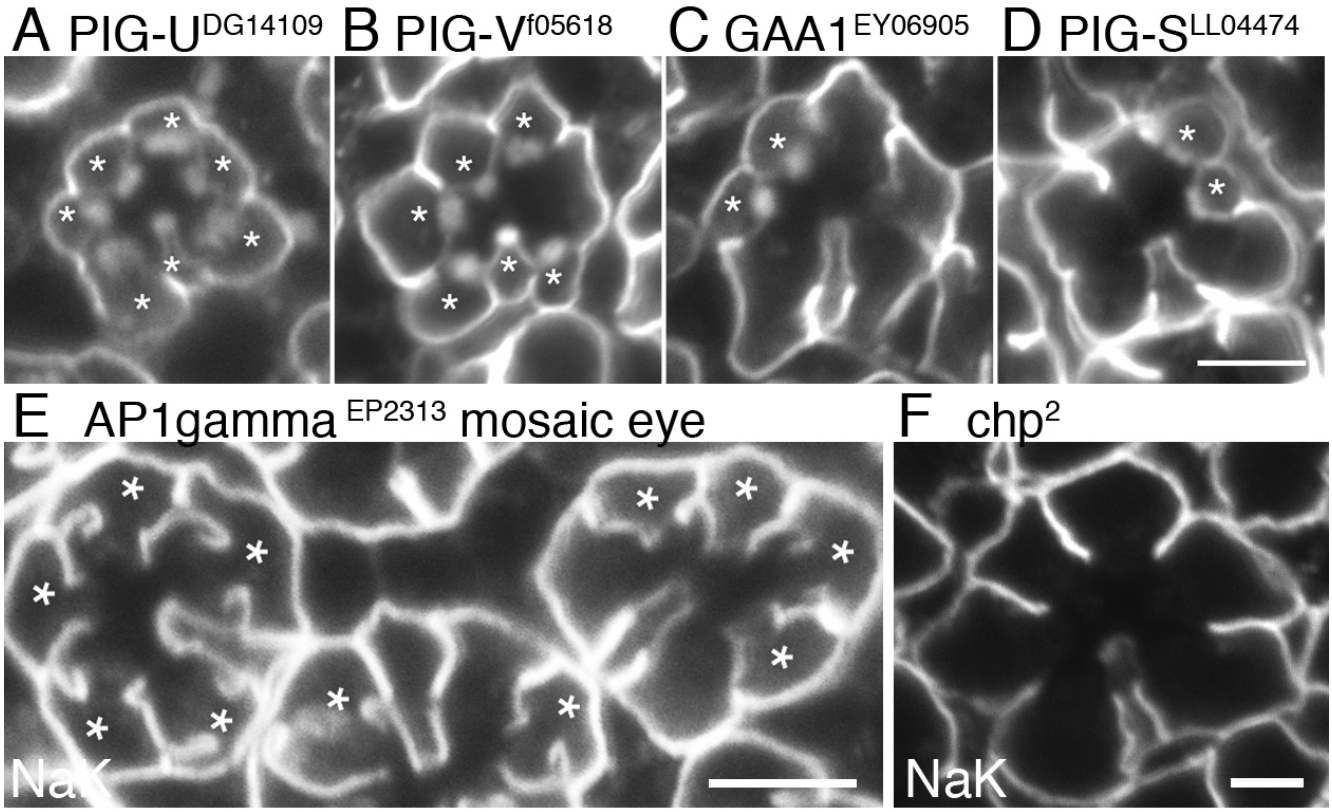


**Fig. S3. Na⁺K⁺-ATPase mislocalization and raft-independent sorting in PIG mutants.** (**A-D**) Immunostaining of Na⁺K⁺-ATPase in the mosaic retina containing both wild-type and PIG mutant photoreceptors. Asterisks show PIG mutant photoreceptors. Scale bar: 5 μm. (**E**) Immunostaining of Na⁺K⁺-ATPase in the mosaic retina containing both wild-type and *AP1γ*$^{e454e6}$ hypomorphic photoreceptors. Asterisks show *AP1γ*$^{e454e6}$ hypomorphic photoreceptors. Scale bar: 5 μm. (**F**) Immunostaining of Na⁺K⁺-ATPase in chp$^{2}$ mutant photoreceptors. Scale bar: 2 μm.

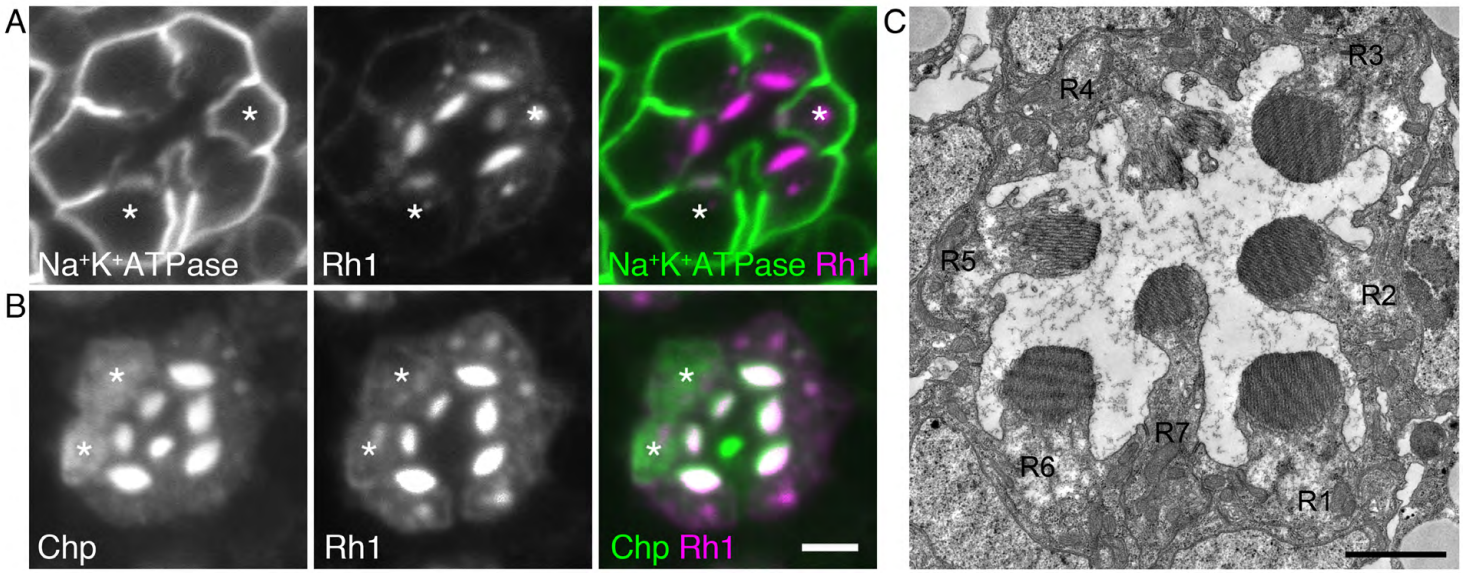


**Fig. S4. Defects of Rh1 and Na⁺K⁺-ATPase transport in partially rescued *PIG-C*$^{f05249}$ photoreceptors.** (**A**,**B**) Immunostaining of late-pupal mosaic retina containing both wild-type and *PIG-C*$^{f05249}$ photoreceptors in which *PIG-C* is expressed only during early eye development. Asterisks show *PIG-C*$^{f05249}$ photoreceptors. Antibodies used are specified below: (A) Na⁺K⁺-ATPase (green) and Rh1 (magenta). (B) Chp (green) and Rh1 (magenta). (**C**) Observation of late-pupal mosaic ommatidium containing both wild-type and *PIG-C*$^{f05249}$ photoreceptors in which *PIG-C* is expressed only during early eye development. R4 and R5 photoreceptors are *PIG-C*-null mutants. Scale bars: 2 μm.

**Table S1. Summary of live-image screening results.** The results of the live-image screening are summarized with the stock numbers of flies and genes potentially affected by the insertions (Chen et al., 2005). The defects judged from the Arr2-GFP pattern were scored for each category, ommatidial pattern defect, rhabdomere morphological defect, and strength of the Arr2-GFP signal in the rhabdomere. +, some phenotype; –, no phenotype; ND, phenotype not described due to severe ommatidia malformation; PCP, planar cell polarity; *, lines confirmed that the Arr2-GFP pattern phenotype is independent of the transposon insertion.

| Stock number | Gene 1 | | Gene 2 | | Cytology | Ommatidia morphological defect | Rhabdomere morphological defect | Apparent Arr2-GFP reduction | Other comments |
|---|---|---|---|---|---|---|---|---|---|
| | CG number | Symbol | CG number | Symbol | | | | | |
| KY111795 | CG2945 | cin | | | 1A1 | - | - | - | |
| KY111968 | CG2945 | cin | | | 1A1 | - | - | - | |
| KY111796 | CG17131 | SP71 | | | 1A5 | - | - | - | |
| KY111940 | CG17131 | SP71 | | | 1A5 | - | - | - | |
| KY111767 | CG16983 | skpA | CG13363 | Suv4-20 | 1B14 | - | - | - | |
| KY111776 | CG16983 | skpA | CG13363 | Suv4-20 | 1B14 | - | - | - | |
| KY111942 | CG18273 | CG18273 | CG3156 | CG3156 | 1B4 | - | - | - | |
| KY111797 | CG3703 | CG3703 | | | 1D2 | + | + | + | |
| KY111760 | CG14779 | pck | | | 2A4 | - | - | - | |
| KY111769 | CG14779 | pck | | | 2A4 | - | - | - | |
| KY111905 | CG14788 | l(1)G0431 | | | 2A4 | - | - | - | |
| KY114354 | CG14813 | _COP | | | 2B12 | + | ND | ND | |
| KY111799 | CG11579 | arm | | | 2B14 | - | - | - | |
| KY111798 | CG3771 | a6 | CG11491 | br | 2B7 | - | + | - | |
| KY111941 | CG3981 | Unc-76 | | | 2C10 | - | - | - | |
| KY111753 | CG3981 | Unc-76 | CG16903 | CG16903 | 2C10 | + | ND | ND | |
| KY111800 | CG3954 | csw | | | 2D1 | + | + | + | |
| KY111763 | CG33950 | trol | | | 3A3 | - | - | - | |
| KY111801 | CG33950 | trol | | | 3A3 | - | - | - | |
| KY114367 | CG33950 | trol | | | 3A3 | - | - | - | |
| KY111741 | CG2621 | sgg | | | 3A8 | + | ND | ND | |
| KY111774 | CG2621 | sgg | | | 3A8 | + | ND | - | |
| KY111938 | CG2849 | Rala | | | 3E5 | - | - | - | |
| KY111773 | CG34412 | tlk | | | 3F1 | - | - | - | |
| KY111804 | CG3665 | Fas2 | | | 4B1 | - | - | - | |
| KY111871 | CG3665 | Fas2 | | | 4B1 | - | - | - | |
| KY111911 | CG3665 | Fas2 | | | 4B1 | - | - | - | |
| KY111943 | CG3000 | rap | | | 4C11 | + | + | ND | |
| KY111802 | CG6998 | ctp | | | 4C13 | - | - | - | |
| KY111805 | CG6998 | ctp | | | 4C13 | - | - | - | |
| KY111880 | CG6998 | ctp | | | 4C13 | + | - | - | |
| KY111962 | CG3564 | CHOp24 | | | 4C7 | - | - | - | |
| KY111755 | CG32763 | l(1)G0045 | CG3201 | Mlc-c | 5A8 | - | - | - | |
| KY111770 | CG32763 | l(1)G0045 | CG3201 | Mlc-c | 5A8 | - | - | - | |

**Table S2. *Drosophila* homologs of human PIG genes.** *Drosophila* homologs of human PIG genes were identified by a search based on the identity of the primary structure and added to the list of human genes encoding enzymes related to GPI biosynthesis and remodeling (Fujita and Kinoshita, 2010).

| | **Mammals** | ***Drosophila*** |
|---|---|---|
| GPI-GlcNAc transferase (GPI-GnT) | *PIG-A* | *CG6401* |
| | *PIG-C* | *CG12077* |
| | *PIG-H* | *CG14463* |
| | *PIG-P* | *CG14550* |
| | *PIG-Q* | *Gpi1* (*CG32578*) |
| | *PIG-Y* | Not found |
| | *DPM2* | Not found |
| GlcNAc-PI de-N-acetylase | *PIG-L* | *CG4433* |
| Inositol acyltransferase | *PIG-W* | *CG9870* / *CG18173* |
| a1,4-mannosyltransferase I (GPI-MT I) | *PIG-M* | *CG9865* |
| | *PIG-X* | *CG30381* |
| a1,6-mannosyltransferase II (GPI-MT II) | *PIG-V* | *veg* (*CG6657*) |
| EtNP transferase I (GPI-ET I) | *PIG-N* | *CG2292* |
| a1,2-mannosyltransferase III (GPI-MT III) | *PIG-B* | CG12006 |
| a1,2-mannosyltransferase IV (GPI-MT IV) | *PIG-Z*(*SMP3*) | *CG3419* |
| EtNP transferase III (GPI-ET III) | *PIG-O* | *CG12263* |
| | *PIG-F* | *CG9376* |
| EtNP transferase II (GPI-ET II) | *PIG-G* (*GPI7*) | *CG2144* |
| | *PIG-F* | *CG9376* |
| GPI transamidase | *PIG-K* | *CG4406* |
| | *GAA1* | *CG3033* |
| | *PIG-S* | *CG31120* |
| | *PIG-T* | *CG11190* |
| | *PIG-U* | *CG13089* |
| Inositol deacylase | *PGAP1* | *CG3160* |
| 2nd EtNP phosphoesterase | *PGAP5* | *CG8455* |
| GPI-phospholipase A2 | *PGAP3* | *CG3271* |
| Lyso-GPI acyltransferase I | *PGAP2* | *CG3876* |